HIGH RESOLUTION SPECTROSCOPY AND HYPERFINE STRUCTURE

Thesis for the Degree of M. S.

MICHIGAN STATE COLLEGE

Robert Carney McBryde

1951

This is to certify that the

thesis entitled

HIGH RESOLUTION SPECTROSCOPY AND
HYPERFINE STRUCTURE

presented by

Robert Carney McBryde

has been accepted towards fulfillment
of the requirements for

Master's degree in Physics

C. D. Hause
Major professor

Date August 2, 1951

O-169

HIGH RESOLUTION SPECTROSCOPY AND HYPERFINE STRUCTURE

by

Robert Carney McBryde

A THESIS

Submitted to the School of Graduate Studies of Michigan
State College of Agriculture and Applied Science
in partial fulfillment of the requirements
for the degree of

MASTER OF SCIENCE

Department of Physics

1951

Grateful acknowledgement is made to Dr. C. Duane Hause for the suggestion of this problem and his invaluable assistance during the experimental and interpretation phases. To Dr. C. Kikuchi for helpful discussions of line breadths and hyperfine structure appreciation is also expressed.

Robert McBryde

TABLE OF CONTENTS

I. Introduction.

In the high resolution investigation of the atomic spectra characteristic of elements having a nuclear spin, spectral lines which otherwise appear to be single are found to be complex groups of closely spaced lines, the hyperfine structure of the transition. Since knowledge of such structure intervals and the information derivable from them - nuclear spin and magnetic moment, nucleus-electron interaction constants - leads to a better understanding of atomic structure, the measurement of hyperfine structure is of importance. Hyperfine structure intervals are often small fractions of a wave number (cm^{-1}) and hence light sources which produce lines having breadths smaller than these intervals are required; actual resolution of structure being accomplished using Fabry-Perot and Lummer-Gehrcke plate interferometers or reflection and transmission type echelons.

A knowledge of the physical conditions influencing spectral line breadths and control of their effects and the techniques of using interferometers as spectrometers are necessary. A summary will be given in this report of such factors and the type of broadening produced, design and construction details of a hollow cathode discharge source, and an indication of the theory underlying interferometer spectrometers - the Fabry-Perot etalon and Lummer-Gehrcke plate - for use with such a

source. The theory of hyperfine structure as arising from nucleus-electron interaction will be given and an attempt will be made to investigate the hyperfine structure of the $^2D - ^2P$ multiplet in Cu. In addition, qualitative measurements of the influence of source operating conditions - gas pressure, cathode temperature and discharge tube current - on the line breadth as observed in fringe width will be presented.

II. Line Width.

A. In order to reduce spectral line widths as produced by a source, the various physical conditions influencing such line widths must be analyzed and these factors utilized in the design of a suitable source. There are, in general, five factors influencing line width; these are,

1. Radiation damping	Natural width
2. Doppler effect	Doppler width
3. Collision damping	Collision width
4. Pressure effects	Pressure width
5. Stark effect	Stark width

Of these five effects the following statements may be made:

1. Only the natural and doppler widths are independent of the density of the emitting or absorbing atoms, the remainder depending directly upon the density.
2. Quantitative discussions are possible from a theoretical viewpoint for only the natural and doppler widths; only a rough qualitative explanation being possible for the others.
3. Collision and pressure width mechanisms are not fully understood; many differing views are evident in literature.

B. Natural width[1]

Classically, the natural width of a spectral line is due to radiation damping; a vibrating, therefore radiating, electric charge

continually loses energy and, as a result, the amplitude of vibration decreases while the frequency of vibration, ν_0 , remains constant. Assuming an electron which may vibrate about an equilibrium position subject to a linear restoring force, a fourier analysis of the electric moment of the charge as a function of time t reveals that the radiation is not monochromatic but has a definite frequency distribution

(1) $$I(\nu) = \frac{\gamma/2\pi}{(\nu_0 - \nu)^2 + \left(\frac{\gamma}{2}\right)^2}$$ The quantity γ is given by

(2) $$\gamma = \frac{4\pi e^2 \nu_0^2}{3 m c^3} \ sec^{-1}$$ where m and e are the mass and charge of the particle in question. The form of this distribution is indicated in Fig. 1.

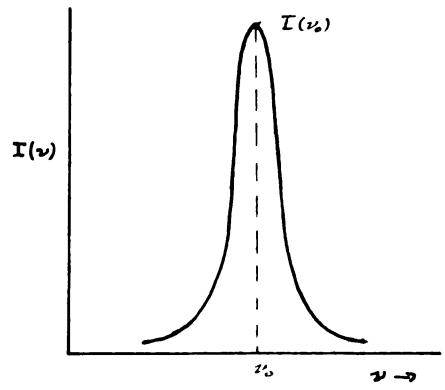

Fig. 1

The half width* of this frequency distribution is given by the constant γ , since setting $I(\nu) = I_0/2$, half the maximum intensity at $\nu = \nu_0$, and solving for ν gives $\nu = \nu_0 \pm \gamma/2$. Notice that γ

* By half width we shall mean the width of the frequency distribution curve at half maximum intensity.

is a constant and has the value

$$\gamma = \frac{4\pi e^2}{3mc^2} \text{ cm} \qquad \text{or}$$

(3) $\gamma = 1.17 \times 10^{-4}$ A , a value which is independent of wavelength. Actually, observations of the natural width indicate that it is not a constant but depends upon wavelength.

This nondependence of the natural line width upon wavelength is not realised when the problem is considered quantum mechanically. Here the energy levels, E_1 and E_2, between which the transition occurs are not infinitely sharp but have finite widths ΔE_1, and ΔE_2 which are given by the Heisenberg uncertainty principle,

$\Delta E \, \Delta t \sim \frac{h}{2\pi}$, Δt being thought of as the average time spent by the atom in that particular energy state. Analysis of this condition shows that the total line width is the sum of the term widths of the two levels; $\Upsilon = \gamma_1 + \gamma_2$ and is given by the relation

(4) $\gamma = \frac{4\pi e^2}{3mc^2} \left(\sum_1^k \nu_{1k}^2 f_{1k} + \sum_1^i \nu_{1i}^2 f_{1i} \right)$ where ν_{1k} and f_{1k} are the frequency and "oscillator strength" corresponding to the transition $E_1 \longleftrightarrow E_k$, the summation being over all energy states lower than E_1. Although the actual values for the oscillator strengths are unknown in the general case, the line width will depend upon the wavelength (frequency) of the transition and is not a constant as predicted classically.

C. Doppler width[1,2]

In the classical Doppler effect, the frequency of radiation ν

emitted or absorbed by an atom in motion is

(5) $\nu = \nu_0 (1 - v_x/c)$ where ν_0 is the frequency of radiation from the source and v_x the component of velocity in the direction of propogation of the light. Clearly then, in a gas with a random or thermal motion of the atoms or molecules this change of frequency with the nature of motion of a particle will produce a broadening of the spectral lines. In the case of a discharge in a gas the particle velocities, and since there is a preferred direction of motion an actual shift in the spectral line will be observed.

Suppose light from a uniform, continuous source passes through a gas, the molecular or atomic velocities being only those due to thermal agitation. If all of the gas molecules were at rest the frequency of the light absorbed would be ν_0 (assuming a gas of one type molecule only), a very nearly monochromatic frequency. If the molecules are in thermal equilibrium the frequency of the light absorbed is ν as given by (5) and the fraction of the total intensity absorbed will be proportional to the number of molecules having velocities in the interval v_x to $v_x + dv_x$. Assuming a Maxwell-Boltzman distribution of velocities, the number of molecules having this range of velocities is

(6) $$dN_{v_x} = N \sqrt{\frac{M}{2\pi RT}} \exp\left(-\frac{M}{2RT} v_x^2\right) dv_x$$

where N is the number of molecules having mass M at an absolute temperature T, R being the gas constant.

The frequency distribution function of the absorbed light is

given by

$$(7) \qquad I(\nu) = \sqrt{\frac{Mc^2}{2\pi RT\nu_0^2}} \exp\left[-\frac{Mc^2}{2RT\nu_0^2}(\nu-\nu_0)^2\right]$$

equation (5) being used to eliminate v_x and dv_x. The form of this distribution is indicated in Fig. 2.

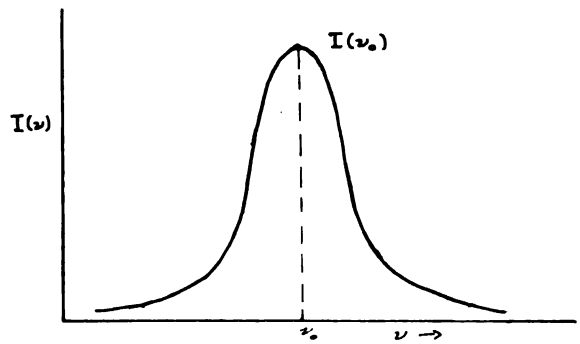

Fig. 2.

The half width of this frequency distribution is

$$\Delta\nu_{1/2} = 2\sqrt{\log 2}\sqrt{\frac{2RT}{Mc^2}}\nu_0 \text{ or in terms of wavelength}$$

$$(8) \qquad \Delta\lambda_{1/2} = 2\sqrt{\log 2}\sqrt{\frac{2RT}{Mc^2}}\lambda_0$$

λ_0 being the wavelength corresponding to a frequency ν_0. From the expression for the doppler width, it is evident that $\Delta\nu_{1/2}$ depends upon the wavelength; $\Delta\nu_{1/2}$ being more pronounced for larger λ. Unlike the natural line width, the doppler breadth may be experimentally controlled by merely varying the temperature T of the absorbing or emitting atoms. Such a practive is very necessary for lighter atoms dne to the dependence upon the inverse root of mass.

D. Collision width

Considerable controversy over the mechanism of collision broadening exists. There is the impact theory of Lorentz which visualizes the

radiation ν_o emitted or absorbed by an atom as being terminated during the time of collision with another atom, this finite wave train giving a frequency distribution of intensity. Statistical theory predicts a collision broadening due to a perturbation of the energy levels of a radiating atom by the presence of the remaining atoms, the perturbation energy being a function of the positions of the perturbers. A brief discussion of each of these methods of attack is given.

The impact or Lorentz theory of collision broadening makes the assumptions:

1) Energy is emitted or absorbed only during the time between elastic collisions, the radiation process being resumed after collision with the same frequency and possibly a change in phase;

2) The time of collision is very short compared with the time between collisions.

The radiating atom is pictured as colliding elastically with other atoms, the amplitude of radiation emitted during the period between collisions being of the form $A e^{i\omega_o t}$. Using the form of the amplitude as

$$(9) \qquad A(t) = \begin{cases} 0 & t > \tau \\ A_o e^{i\omega_o t} & o < t < \tau \end{cases}$$

the fourier integral of this function yields for the amplitude frequency distribution $f(\omega)$ the result

$$(10) \qquad f(\omega) = \frac{A_o}{\sqrt{2\pi}} \; \frac{e^{i(\omega_o - \omega)\tau} - 1}{i(\omega_o - \omega)} \; .$$

Since in a gas the radiators are incoherent, the frequency distribution

of intensity is proportional to $\sum |f(\omega)|^2$ and is given by

(11) $I'(\omega) = C \frac{\sin^2 \left(\frac{\omega_0 - \omega}{2}\right)\tau}{(\omega_0 - \omega)^2}$ for a single

particle. Since Maxwell-Boltzman statistics obtain for the gas particles, the number of molecules which have a time τ between collisions is $e^{-\tau/\tau_0}$, τ_0 being the collision frequency. On this assumption of a Maxwell-Boltzman distribution of speeds for the gas molecules, τ_0 is given by

(12) $\tau_0 = \frac{1}{\sqrt{2}\,\pi\sigma^2 m \bar{v}}$

σ - collision diameter of molecule

m - density of molecules

$\bar{v}$ - mean speed of molecules.

The total intensity for a frequency ω is then

$$I(\omega) = C \int_{-\infty}^{\infty} e^{-\tau/\tau_0} \frac{\sin^2 \left(\frac{\omega_0 - \omega}{2}\right)\tau}{(\omega_0 - \omega)^2} \, d\tau$$ which is of the form

(13) $I(\omega) = \frac{I(\omega_0)}{1 + \tau_0^2 (\omega_0 - \omega)^2}$ where $I(\omega_0)$ is the

maximum intensity. From this intensity frequency distribution, the half width is seen to be

(14) $\Delta\nu_{1/2} = \frac{1}{\pi\tau_0}$ where τ_0 is given by (12) and

since $\bar{v} = \sqrt{\frac{8kT}{\pi m}}$ becomes

(15) $\Delta\nu_{1/2} = 4\sigma^2 m \sqrt{\frac{kT}{\pi m}}$. Hence the line breadth on the Lorentz theory of impact broadening depends directly upon the density of molecules and also upon the temperature and mass of the absorbing or radiating molecules.

Although this theory gives a quantitative expression for $\Delta\nu_{1/2}$, its dependence upon a collision diameter σ is misleading. If observed line breadths are used with (15) to calculate σ the result does not agree with the molecular diameters as determined from viscosity measurements; in almost all cases a factor of from 2 to 5 exists between σ as determined spectroscopically and that from viscosity effects. This points the need for some other mechanism of collision broadening, the statistical theory.

In the statistical theory of collision broadening[3] the instantaneous distribution of molecules in space is analyzed, the energy levels of the radiating or absorbing molecule being perturbed by interaction with neighboring molecules. The frequency of a spectral line arising from a transition between any two levels will then be diffused over an interval corresponding to the range of such intermolecular perturbations as are involved. In the range ν to $\nu + d\nu$ the intensity of a line is therefore proportional to the statistical probability that the energy difference of the two levels involved lies between $h\nu$ and $h(\nu + d\nu)$. For low pressures this interaction will be predominantly one with nearest neighbors and weighting the frequency shift $(\nu - \nu_0)$ in this case according to the probabilities of the appropriate intermolecular separations, the intensity frequency distribution $I(\nu)$ is found to vary inversely with $(\nu - \nu_0)^2$. Although this distribution has an infinity at resonance, $\nu = \nu_0$, the general form away from resonance is similar to the symmetric distributions already encountered.

Holstein[4] in a paper "Pressure Broadening of Spectral Lines" shows that the impact theory of collision broadening is valid near resonance conditions, that is near the line center, and also that the statistical theory is valid for frequencies $\nu \gg \nu_0$, in the wings of the spectral line. In addition, the intensity frequency distribution as predicted by both the impact and statistical theory treatments are continuous; that is, the distribution function for the center of the spectral line passes smoothly into that for the wings with no discontinuity in the function or its first derivative.

Collision broadening of spectral lines, for low pressures, results in a symmetrical intensity frequency distribution similar to those for natural and Doppler breadths as in Fig. 1 and 2.

E. Pressure broadening.

Increasing the density of the molecules surrounding a given emitting or absorbing molecule has the effect of producing an asymmetrical broadening and an actual shift in the center of the spectral line, the shift being of the order of several angstroms in the case of extreme pressures. In all cases the asymmetry in line shape is to the red, to lower frequencies. A qualitative explanation of the asymmetrical broadening is found on extension of the impact theory of collision broadening to take into account the altered radiation emitted or absorbed during the actual collision. One now uses for the amplitude function $A(t)$, analogous to (9),

$$(16)\quad A(t) = \begin{cases} 0 & t > \tau \\ A_1 e^{i\omega_1 t} & 0 < t < \tau_1 \\ A_2 e^{i\omega_2 t} & \tau_1 < t < \tau \end{cases}$$

where τ_1 is the period between collisions and $\tau - \tau_1$ the duration of the collision process. An intensity frequency distribution function, $I(\omega)$, should now be possible by proceeding as before in obtaining the fourier integral of (16) and, using this, determining $I(\omega)$. However, the expression obtained for $f(\omega)$ is extremely complex and, unless the frequencies between and during collisions are known, does not indicate the asymmetry in line shape. Only in the extreme case of near instantaneous collisions (relative to the time τ_1) may $I(\omega)$ be obtained. In this case (13) is obtained since a low pressure is assumed in making $\tau_1 >> (\tau - \tau_1)$.

Recently Margenau[5] has investigated the effects of pressure broadening on a statistical basis for any interaction law which varies inversely as the n'th power of the particle separation. The distance between two energy levels involved in a transition is a function of the unperturbed energy ϵ_0 and the potential due to the surrounding perturbing particles, V where $V = \sum_i V_i$. Hence the statistical treatment demands that the probability of an instantaneous configuration of particles giving $V = \sum_i V_i$ must be determined, this probability giving the spectral line intensity. From this analysis, Margenau finds that the probability $W(V)$ that a total potential V is produced at the emitting or absorbing particle is given by

$$(17) \qquad W(V) = \frac{1}{\pi |V|} \int_0^\infty \exp\left[- \left(\upsilon \frac{V_0}{V} \right)^{3/n} \right] \cos \upsilon \, d\upsilon$$

where V_0 represents the potential energy of two particles at the mean distance of separation and where V_i is assumed to have the form

$V_i = C\, r_i^{-m}\, U(\xi_i)$; $U(\xi_i)$ depending upon particle spin and all other variables other than r_i and in the analysis is assumed to possess a vanishing mean. The important result of this analysis is that the intensity at the center of a pressure broadened line, $W(o)$, is

$$W(o) \propto d^{-m/3}$$ where d is the number density of the particles.

Comparing collision and pressure broadening it is evident that in the former case only nearest neighbors are considered; the interaction of these two closest molecules being treated either as a collision process or from a statistical point of view as to the frequency shift. When higher particle densities are encountered, nearest neighbor interactions are no longer sufficient but the entire assemblage of molecules must be considered, as perturbing a single radiating molecule, the effect being one of a depression of the molecular energy levels. Due to the fact that inner levels are more tightly bound, the depression will be larger for higher, loosely bound states and the resultant spectral lines will be shifted to lower energies, that is to the longer wave lengths. The resultant intensity frequency distribution for pressure broadened spectral lines appears somewhat as indicated in Fig. 3, which may be compared with the symmetrical line shapes of Fig. 1 and 2.

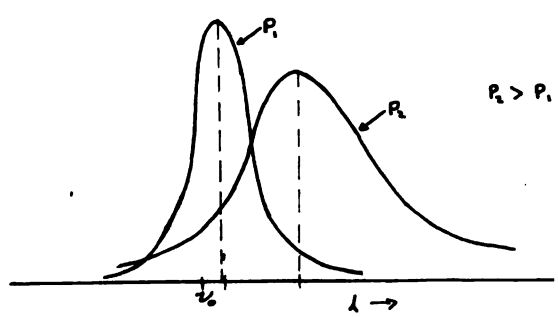

Fig. 3

Although fairly high pressures are required to produce an easily observable line center shift when using low dispersion instruments, when extremely high resolution is employed even moderate pressures give detectable line shifts, a serious defect indeed if quantitative investigations are to be made.

F. Stark breadth.

Analogous to the Zeeman effect in spectral lines, the splitting of a spectral line into numerous components by the action of an external magnetic field upon the angular momentum of an atom or molecule, there is a corresponding effect produced by an electric field, the Stark effect. In the Zeeman effect the total angular momentum of the particle is quantised in the field direction and may take only the values $m_J \frac{h}{2\pi}$ where the magnetic quantum number m_J takes the values

$$m_J = J, J-1, \ldots -J \quad ; \text{ each orientation}$$

of the angular momentum vector representing a different particle energy. Although the total angular momentum vector is quantized in the electric field direction in the Stark effect, the magnetic quantum number takes the values

$$m_J = 0, \pm 1, \pm 2 \cdots \pm J \quad , \text{ the plus and minus}$$

sign indicating that the particle energy is the same for either orientation: depends only upon the magnitude of m_J .

An exact solution for the effect of an electric field upon the energy levels of a one electron atom is found by solving the Schrodinger equation for the hydrogen atom, the interaction of electric field and atom then being of the form

$\Delta T = AF + BF^2 + CF^3 + \ldots$ where ΔT is the change in term value for a field strength F, A, B and C being constants depending upon the quantum numbers. For low field strengths F, the term value shifts are very nearly given by $\Delta T = AF$ and hence is the first order stark effect; as larger fields are used the second and third order terms become important, these being denoted as the second and third order stark effects.

In a gaseous discharge many ions are formed which, upon collision or close approach, subject emitting or absorbing molecules to very intense electric fields with the result that the observed spectral lines, transitions between these altered term values, will be affected. Since the electric fields produced are not of constant value but vary during the collision or near-collision process reaching a maximum and diminishing once again, the net result on the observed spectral lines should be a symmetric broadening. The electric fields through which the molecules move in a discharge should also produce a broadening of the lines and, in the case of molecules possessing permanent electric dipoles, quadropoles or higher multipoles, collisions or near-collisions between the molecules should have the effect of broadening the lines.

If an average field F is assumed to exist during a collision of two particles, calculation[6] has shown that such a field is given by

(18)
$$F = \begin{cases} a_1 e n^{2/3} & \text{ions} \\ a_2 \mu n & \text{dipoles} \\ a_3 q n^{4/3} & \text{quadropoles} \end{cases}$$

where the a_i are constants, N is the density of the particle, e the electronic charge, μ dipole moment and q the quadropole moment. It will be noted that the "average field" produced by the ions or electric multipoles depend strongly upon the density of particles in the discharge region. From these average fields can be calculated an intensity distribution function, $I(\omega)$, the form of which is similar to that of Eq. (1) and having a half-width $\Delta\nu_{1/2}$ given by

$$\Delta\nu_{1/2} = \begin{cases} 3.25\, A_{i\,max}\, e\, N^{1/3} & \text{ion} \\ 4.54\, A_{i\,max}\, \mu N & \text{dipole} \\ 5.52\, A_{i\,max}\, q\, N^{1/3} & \text{quadropole} \end{cases} \qquad (19)$$

, the quantity $A_{i\,max}$ gives the total spread of the stark levels from the change in term value $\Delta T = AF + BF^2 + CF^3 \cdots$ neglecting the second and third order terms. These relations for the half width give only qualitative agreement when compared to experimentally observed stark broadened lines.

Summarizing then, the factors influencing line widths, nature of the influence - a broadening or shift, type of broadening - a symmetrical or asymmetrical, and the method of reducing or eliminating the effect are given in Table 1.

TABLE I.

Width	Type of effect	Broadening	Remedy
Natural	Broadening	Symmetrical	None
Doppler	Broadening	Symmetrical	Use low temperature
Collision	Broadening	Symmetrical	Use reduced pressures
Pressure	Broadening	Asymmetrical	Use reduced pressures
Stark	Shift-Broadening	Either	Reduce electric field used

III. Hollow Cathode Discharge Source

A. Introductory

Of the several light sources devised which are useful in high resolution investigations, hyperfine structure and rotational structure of molecular band spectra, the hollow cathode discharge tube is simplest in construction and is ideally suited for such work. With this source it is possible to reduce spectral line breadth until, in some cases, the natural width is predominant. In addition to a small line width the hollow cathode discharge tube gives a source of extremely high intensity; sharp spectral lines and high intensity being the chief advantages of such a source.

Essentially, the hollow cathode source is a modified Geissler discharge tube- a source in which an electrical discharge is maintained in a gas at reduced pressure. Paschen[7] modified the Geissler tube by introducing a hollow cathode and found that with correct operating conditions the negative glow receded to the cathode interior and there resulted in a very high intensity glow. The disadvantage of this source was the large Doppler broadening of the spectral lines which masked possible structure. Schuler[8] redesigned the source and removed the cathode to the exterior whence very drastic cooling could be employed. With this possibility of using a low temperature coolant the source became one combining sharp spectral lines and high intensity, the correct combination for the attainment of low resolving limits.

B. General design.

Following design suggestions by Arroe and Mack[9], a hollow cathode source was designed and constructed which incorporated several of their design features. Figure 4 shows in sectional view the hollow cathode discharge tube proper. Since drastic cooling is employed, liquid air for best operation, the main body of the tube is of monel metal, an alloy which retains high tensile strength at low temperatures. Within this body is a glass tube which is closed by a thin glass observation window at the upper end. Within the glass tube at the lower end is placed an aluminum anode, this then being electrically insulated from the cathode. A hollow cathode insert made of copper is placed in the removable base; the vacuum seal at the base is made with a compressed fuse wire ring.

On the gas inlet tube and at the top of the monel body are placed water jackets; the former to maintain the inlet tube at room temperature in order to protect the wax joints and to prevent objectionable frosting of the system, the latter to prevent undue strains on the glass tube and also to keep the apeizon wax at room temperature where its sealing properties are good.

C. Theory of operation.

Although the hollow cathode source may be used to investigate gaseous samples[10], molecular band spectra then being obtained, it is commonly used with pure metallic or metallic oxide samples. As the vapour pressure of such materials are very low, the metal sample is sputtered to form a vapour cloud within the cathode which may then be

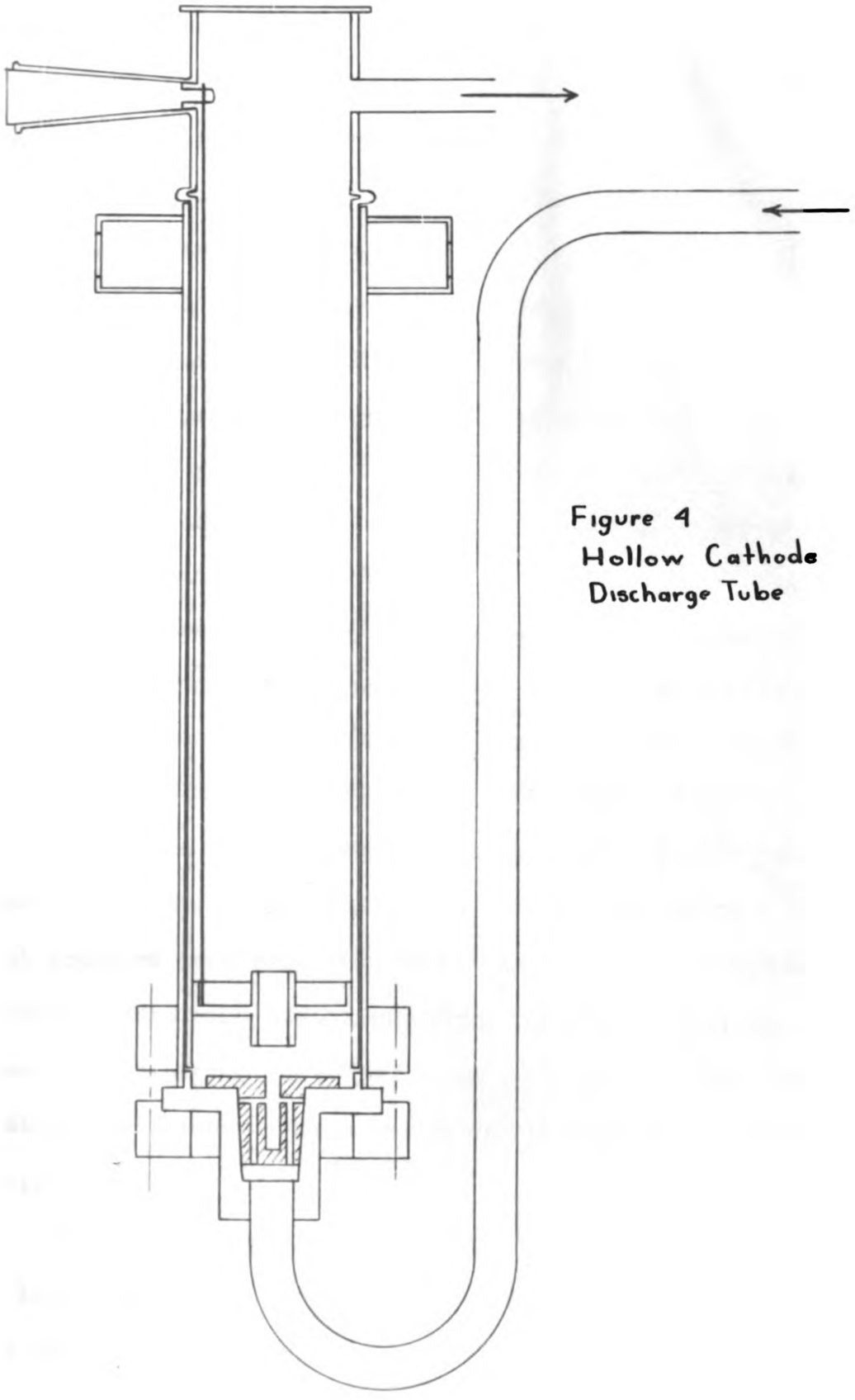

Figure 4
Hollow Cathode
Discharge Tube

excited and its characteristic energies observed.

In such a source an inert gas, argon and helium being commonly used, is passed through the discharge region at reduced pressure. Applying a potential between the anode and hollow cathode initiates a typical gaseous discharge. As the operating conditions of gas pressure and voltage are altered the discharge positive glow disappears while the negative glow becomes prominent and recedes to the cathode interior; the negative glow then assuming a very high intensity. Under these conditions the positive ions of the gas formed in the discharge are urged toward the cathode and upon striking the interior walls of the cathode sputter any material there; that is, a local evaporation of the surface occurs and a vapour cloud is formed. Due to the mechanism of the discharge large numbers of carrier gas atoms are excited to metastable energy states which, since the atoms are unaffected by the electric field, accumulate about the cathode. These metastable atoms still possess energies of 19.7 volts for helium and 11.5 volts for argon. Collisions between these atoms and those of the vapour cloud result in a complete transfer of potential energy of excitation from the metastable atom to the vapour atom, much potential energy being transformed to kinetic energy of motion and, most important, potential energy of excitation. The excited vapour atoms then return to the ground state radiating their characteristic frequencies.

The observed sample spectra should consist of the arc or spark excited lines depending upon whether He or A carrier gas is used. Due to the fact that the carrier gas ions are returned to the ground state without radiating energy, no evidence of the carrier gas spectrum should be

observed. At least the intensity of such lines will be very small relative to the sample spectra if occuring at all. Also, the vapour cloud is at the temperature of the coolant as is the carrier gas and hence Doppler broadening of the spectral lines will be entirely determined by the coolant temperature.

D. Electrode design.

Electrode design in the hollow cathode source is the key to successful operation and to the proper elimination or reduction of controllable line breadth. By proper design the operating conditions - gas pressure and electrode potential - may easily be controlled; rare or minute samples may be used due to recoverability of sample and a maximum utilization of gas ions is effected.

1. A maximum utilization of ions formed in the discharge is secured since the electric field direction is such as to urge the ions to the cathode interior. In Figure 5 is a diagram of the electrodes, the solid lines indicating approximately the equipotential traces, dotted lines the electric field.

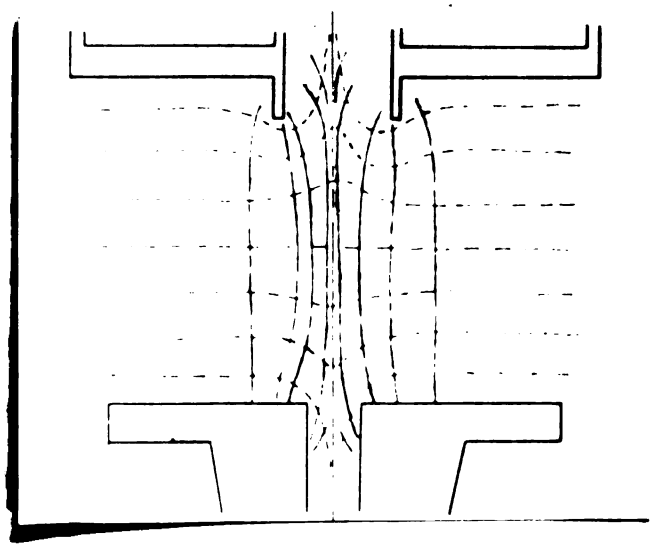

Fig. 5. Equipotential and electric field line traces of electrodes.

Obviously then ions formed in the anode interior will be directed downwards and "focussed" by the electric field so that nearly all enter the cathode. A maximum sputtering will then occur from the cathode interior wall and hence placing a sample of the material under investigation in this region insures that a vapour cloud of sputtered atom will be formed which may undergo excitation. This focussing action occurs only when the discharge is initiated. During actual operation space charge effects about the cathode may drastically change these conditions.

2. With such economy in utilizing the ions for sputtering, extremely small samples of material may be used since the ions may be concentrated within a very small area, depending upon the cathode diameter. An adequate vapour pressure of the material may then be obtained in order that sufficient intensity is available for observations. This feature of small sample size recommends the hollow cathode source for use with rare elements or with the now available enriched isotopic samples.

3. Referring again to Figure 5 it is noted that the carrier gas enters the hollow cathode near the upper end, the gas then accumulates at the cathode opening and forms a protective umbrella over the cathode. This gas umbrella serves to prevent the vapour cloud of atoms from leaving the cathode thus assuring future sample recovery. Placing the anode near the cathode forces the carrier gas to flow through the central cylindrical region of the anode and escaped vapour atoms are deposited here. Thus in case of rare or enriched samples almost complete recovery is possible.

E. Gas system and power supply.

In conjunction with the discharge tube proper there is associated a gas system which allows the carrier gas to flow through the discharge region at a constant reproducible pressure. In addition provision for reducing the cathode temperature is made. Figure 7 and overlay show the complete hollow cathode discharge source and gas flow.

The essential components of the gas system are a high pressure reservoir of gas, leak type reduction valve, discharge tube and high vacuum sink. Lecture bottles of A and He at 1600 psi furnish the carrier gas, this pressure being reduced to 20 psi by a Hoke reduction valve. In the discharge tube proper the gas pressure is controlled by means of tapered leak valves the design of which is indicated in Figure 6. These valves consist of a male taper which may be made to seat snugly or loosely into a corresponding female taper, the flow of gas then being completely adjustable. An O-Ring furnishes the thread end seal. The two valves control the flow rate of gas in and out of the discharge tube and hence control the gas pressure. Gas pressure within the discharge region is indicated on a Hg manometer situated between the discharge tube and outlet valve. Evacuation of the system is accomplished with a Cenco Megavac rotary oil pump running continuously.

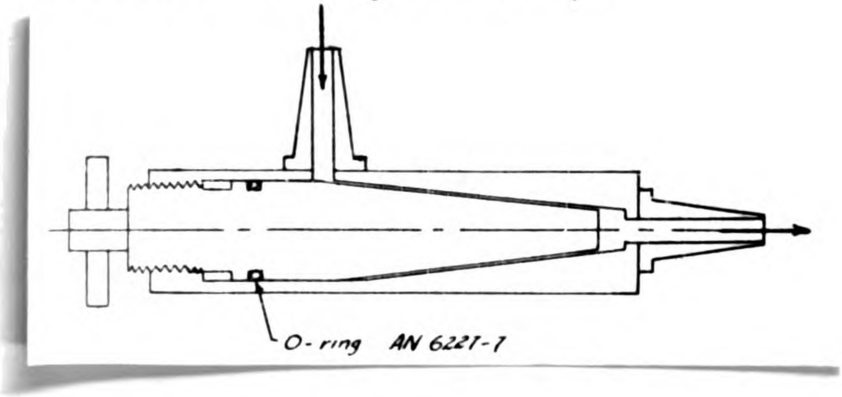

Figure 6.
Leak valve.

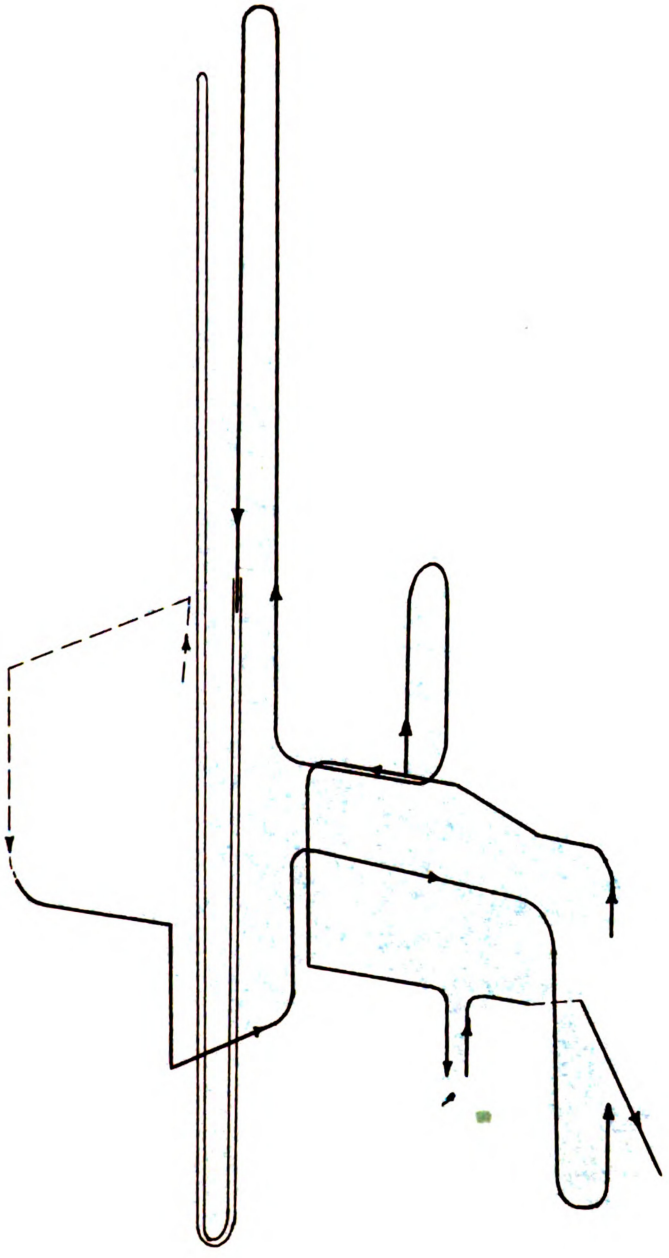

Carrier Gas Flow Diagram.

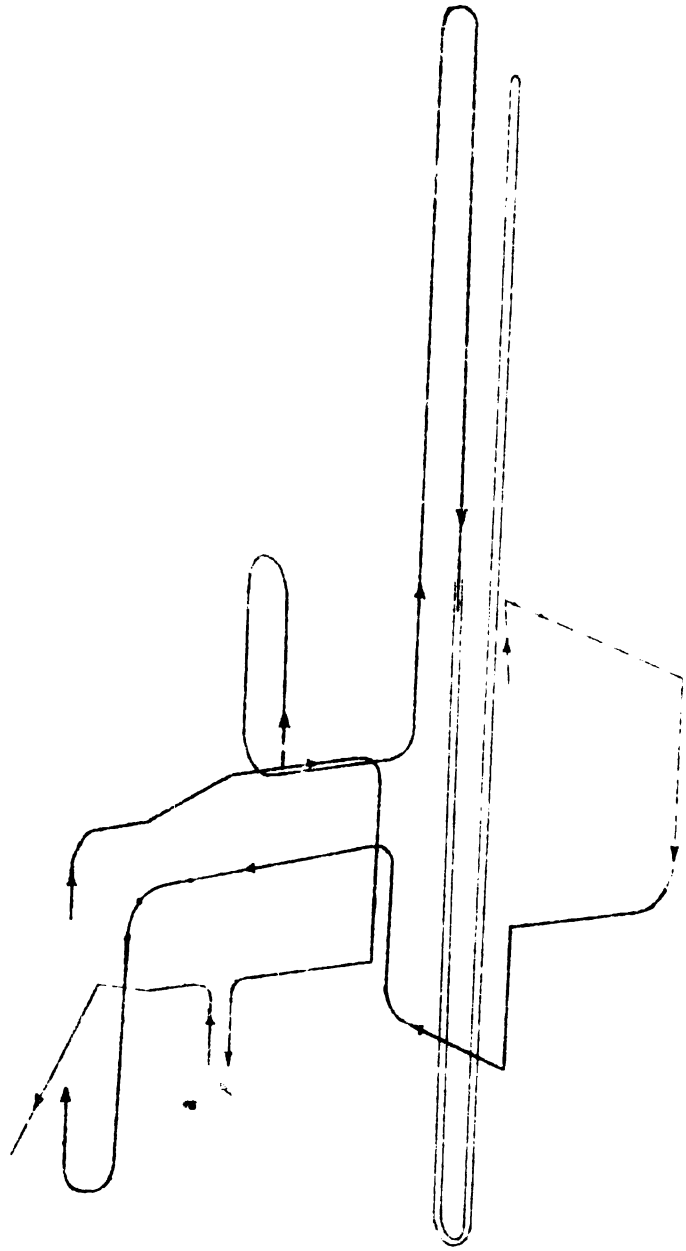

Figure 7

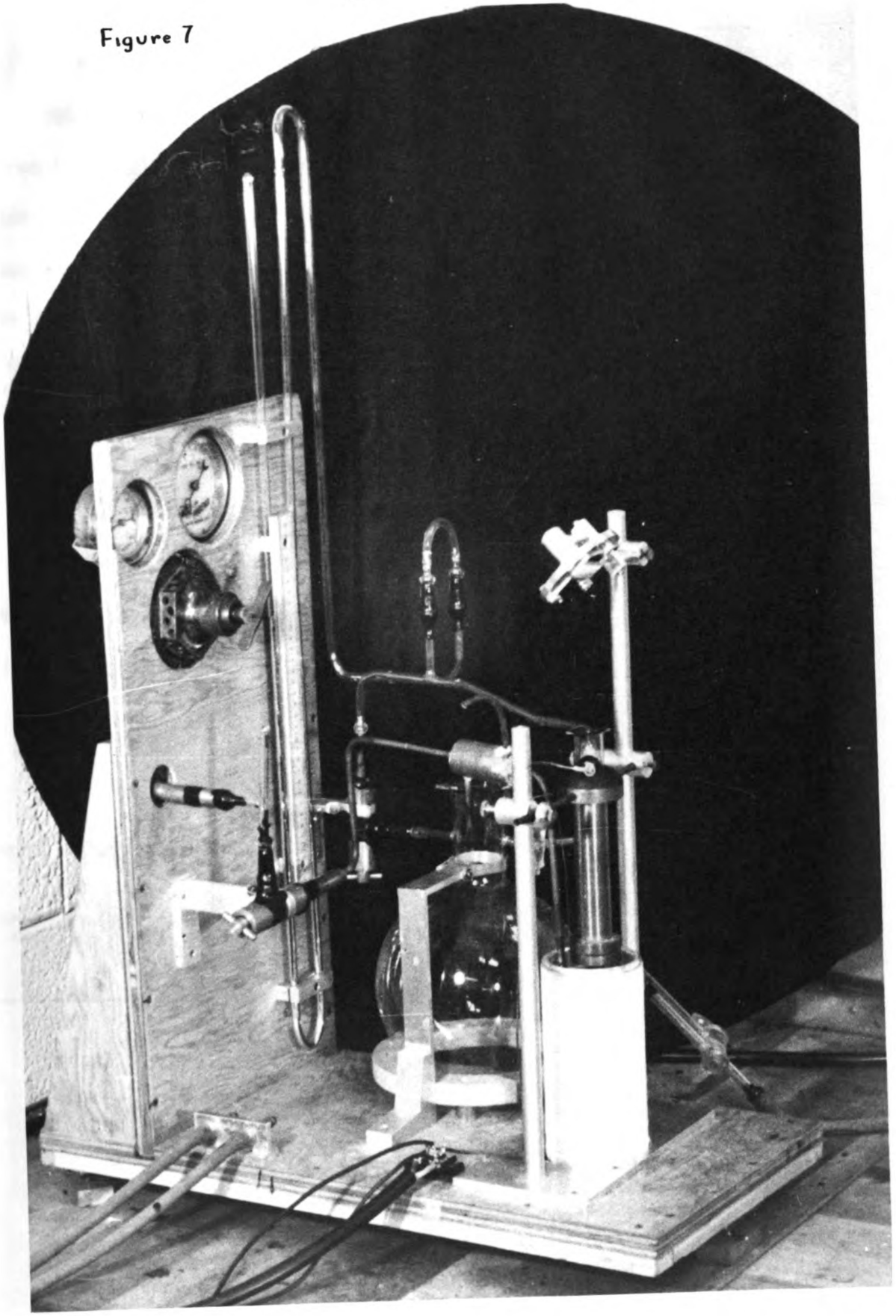

To supply the necessary power for operation of the discharge tube a 2300 volt 1.2 kw filtered full wave rectifier is used, the circuit diagram being given in Figure 8. Since the cathode is electrically connected to the metal portions of the apparatus, the anode is operated above ground potential; no shocks then result to operator. In order to facilitate starting the discharge 2700 ohms resistance is placed in series with the discharge tube. Since the tube resistance is very high at first almost the entire applied potential is across the electrodes but as the discharge commences the tube resistance decreases to about 800 ohms and only about one fourth of the applied potential is across the electrodes during operation. This ballast resistance has the effect of stabilizing the current flow, small fluctuations in tube resistance do not affect the total resistance appreciably and more nearly constant current flow results.

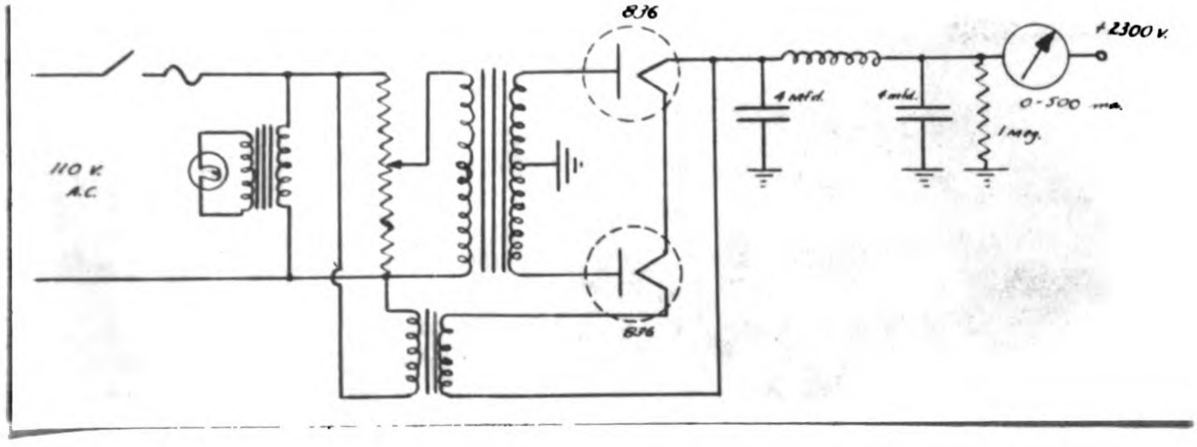

Figure 8. Power Supply.

IV. General Theory of High Resolution Spectroscopy[11]

A. Introductory

High resolution spectroscopy as the term implies is concerned with attaining high resolving powers (low resolving limits) in order that hyperfine structure in spectral lines may be accurately analyzed. The principle involved is that of interference properties of coherent light waves. Interference type optical instruments are chosen which utilize high orders of interference and produce interference fringes of very narrow breadth; these instruments meeting these requirements being the

1. Fabry-Perot interferometer,
2. Lummer-Gehrcke plate,
3. Reflection and
4. Transmission echelons. Of these only the first two receive common application and are the instruments utilized in the detection of hyperfine structure in copper reported here.

Since with an instrument of moderate dispersion hyperfine structure is not completely resolved, the group appearing as a single broadened line, an interference type instrument as listed above is used in order to separate the components. With each of these interferometers a single wavelength of radiation λ will produce a set of characteristic interference fringes. If two wavelengths λ and $\lambda + \Delta\lambda$ are present there will be two superimposed fringe patterns, one corresponding to each wavelength, which are of slightly different size. In practice radiation from a suitable source - one giving sharp spectral lines so that possible

structure is not masked - is first passed through one of these interferometers and then through a suitable dispersing agent, constant deviation spectrometer, monochromator, etc., the resultant observed spectrum will consist of interference fringes normal to the direction of dispersion for each of the source spectral lines. Investigating the interference fringes of each wavelength for fringe components gives indication of the presence of hyperfine structure and analysis of these fringe separations allows the wavelength differences between the components to be determined.

A brief consideration of the theory and use of the Fabry-Perot and Lummer-Gehrcke plate will be given along with methods of reduction of fringe patterns to obtain component separations.

B. Fabry-Perot interferometer.

The Fabry-Perot interferometer is essentially a plane parallel air plate having highly reflecting surfaces; the interference pattern being formed by the recombination of partial waves from a plane wave undergoing successive multiple reflections within these surfaces. From the figure the phase difference between two consecutive partial rays is

$$(1) \quad 2\pi\varphi = 2\pi\left[\frac{2t}{\lambda_a}\cos\varphi - \frac{2t}{\lambda_g}\tan\varphi\sin\varphi\right]$$

where φ is the order number of interference. Since $\lambda_g = \lambda_a m_g$ and $m_g = \sin\varphi/\sin\psi$, the order number becomes

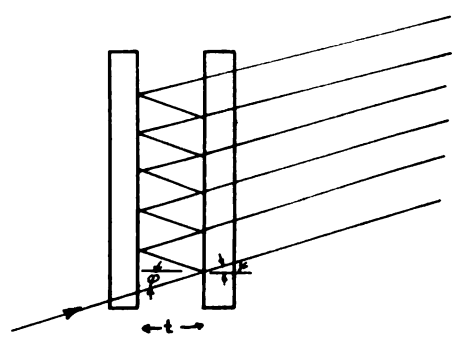

$\varphi = \frac{2t}{\lambda_m} \cos\varphi$. Integral values of φ will correspond to maximum of intensity in the pattern and as $\varphi = \varphi(\varphi)$ each of the integral values of φ correspond to an angle of incidence φ_i ; hence all rays incident at an angle φ_i will produce an intensity maximum in the field, the interference pattern then being composed of concentric rings. Since φ changes by unity in going from one fringe to the next the wave number change is just $\Delta\nu = \frac{1}{2t}$ near the interference pattern center.

If at every incidence upon the reflecting surfaces a portion σ of the amplitude (assuming for simplicity $A = 1$) is transmitted and ρ reflected then the amplitude of the k'th partial wave will be $\sigma^2 \rho^{2(k-1)}$ or in terms of the intensity coefficients s and r , the transmission and reflection power of the surface, $s\, r^{(k-1)}$. Hence at a given point in the focal plane of the projecting lens, the amplitude of vibration is the sum of the individual waves: $s e^{i\omega t}$, $s r e^{i(\omega\tau - 2\pi\varphi)}$, $s r^2 e^{i(\omega\tau - 4\pi\varphi)}$, . . . where $\frac{\omega}{2\pi}$ is the light frequency, τ the time and $2\pi\varphi$ the phase difference between successive waves. Because of the small angles of incidence this summation is essentially an infinite one, hence the resultant amplitude A is given by

$$A e^{i\omega t} = s e^{i\omega\tau} \sum_{1}^{\infty} k\, r^{(k-1)}\, e^{-i2\pi\varphi(k-1)}$$

$$= s e^{i\omega\tau} \frac{1}{1 - r e^{-i2\pi\varphi}} \quad .$$ The observable intensity $I = A \cdot \bar{A}$ and hence is

$$(2) \qquad I(\varphi) = \frac{s^2/(1-r)^2}{1 + \frac{4r}{(1-r)^2} \sin^2 \pi\varphi}$$

which for φ = integral is $I_{max} = \frac{s^2}{(1-r)^2}$ and φ = integral $+ \frac{1}{2}$,

$I_{min} = \frac{a^2}{(1+r)^2}$. Since φ is a function of the interference ring diameters, along these diameters $I(\varphi)$ fluctuates between these values of I_{max} and I_{min} . As r becomes larger, a higher reflecting power, this difference in maximum and minimum intensity becomes greater and the width of the individual fringes decreases.

Using a lens of focal length f to produce the interference fringes of diameter D_i , the $\cos\varphi_i$ term becomes $\cos\varphi_i = \left(1 - \frac{D_i^2}{8f^2}\right)$ and hence the order number φ is

(3) $\varphi = \frac{2t}{\lambda_a}\left(1 - \frac{D_i^2}{8f^2}\right)$. If then two wavelengths λ_1 and λ_2 are present each will produce its characteristic interference pattern, the diameters D_{1i} and D_{2i} being slightly different. It is this property of an interferometer which allows it to be used as a resolving instrument for by reducing the instrumental fringe width, increasing the surface reflecting power, hyperfine structure in the spectral lines may be observed as slightly displaced fringe components.

The resolving power of such an instrument may be obtained by assuming that two overlapping fringes of equal intensity will be just resolved when the ratio of minimum to maximum intensity in the combined intensity distribution is 0.8106 ($8/\pi^2$); this being the Rayleigh criterion. Then the resolving power becomes

$R.P. \equiv \frac{\lambda}{\delta\lambda} = 2.98\frac{r^{1/2}}{(1-r)}\varphi$ a function of the interference order and surface reflection coefficient. This resolving power may be increased simply by increasing the plate separation, - increasing φ , - and increasing the reflection power of the surfaces.

Deduction of wavelength separations of hyperfine structure components from observed fringe patterns depends upon the fact that the order number p is a function of D_i^2 and between consecutive fringed there is a constant difference ΔD_j^2. Hence calling the order of interference at the pattern center P, $P = p_0 + \epsilon$ where p_0 is the first fringe order number and ϵ is a fraction of an order number; ϵ being given by $\epsilon = \frac{D_i^2}{\Delta D^2} - i$. Hence for a two component structure, λ_a and λ_b, the central order numbers are P_a and P_b. Therefore $P_a = p_a + \epsilon_a = \frac{2t}{\lambda_a} = 2t\nu_a$, $P_b = p_b + \epsilon_b = 2t\nu_b$, where ν is in cm^{-1}. The wave number difference is then

$$\nu_b - \nu_a = \frac{1}{2t}(p_b - p_a) + \frac{1}{2t}(\epsilon_b - \epsilon_a)$$

$$(4) \qquad \Delta\nu = \frac{1}{2t}(p_b - p_a) + \frac{1}{2t}\left(\frac{D_{bK}^2}{\Delta D_b^2} - \frac{D_{aK}^2}{\Delta D_a^2}\right)$$

By taking several photographs of the fringe patterns at different values of t the order number difference $p_b - p_a$ may be determined and hence the wave number separation calculated. Reduction of fringe patterns to give component separations are more involved for a larger number of components and hence for methods of reduction and attainment of accurate values reference is made to S. Tolansky, High Resolution Spectroscopy and also to K. W. Meissner, Journal of Optical Society of America, 31, 405 (1941) and 32, 185 (1942).

C. Lummer-Gehrcke plate.

The Lummer-Gehrcke plate interferometer depends for its action upon the fact that the reflecting power of a surface is very large for angles of incidence near the critical angle. In order to secure such reflecting powers without the accompanying absorption as in the case of

metallic films a plane wave is made incident upon a plane parallel plate of glass or quarts in such a manner that the resultant internal reflections are at nearly the critical angle. In such a case, as illustrated in the diagram,a small portion of the wave is transmitted and the majority reflected at each incidence. If the successive emergent waves are brought to a common focus by using a lens as indicated a characteristic interference pattern will be produced which consists of parallel fringes, the spacing of which decreases as the distance from fringe center increases.

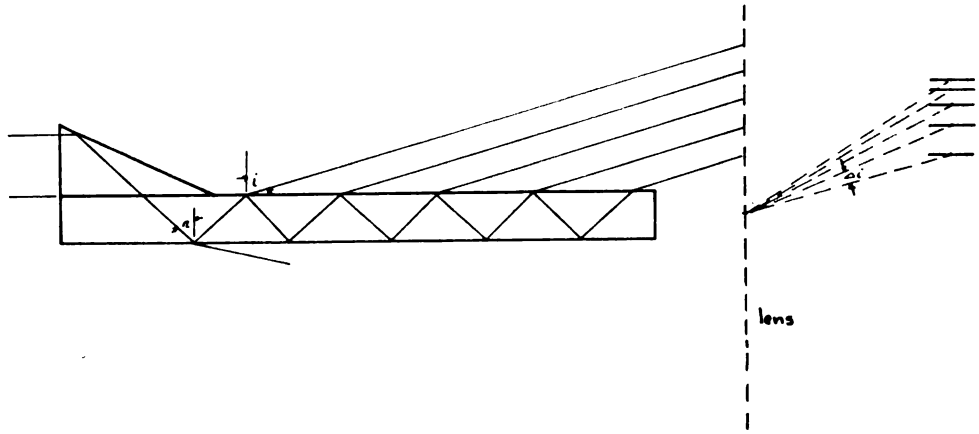

For a Lummer plate of thickness t, length l and refractive index μ the necessary condition for constructive interference of the coherent partial waves is that the path difference be

(5) $2\mu t \cos r = m\lambda$ where m is an integer. From the definition of μ, $\mu \sin r = \sin i$, the relation for costructive interference becomes

(6) $2t\sqrt{\mu^2 - \sin^2 i} = m\lambda$. Denoting the angle between consecutive fringes by Δi, Δi is found by squaring and and differentiating (6) and is $\Delta i = -\frac{m\lambda^2}{2t^2 \sin 2i}\Delta m$ or

since $\Delta m = 1$

$$(7) \quad \Delta i = -\frac{m\lambda^2}{2t^2 \sin 2i} = \frac{-\lambda\sqrt{\mu^2 - \sin^2 i}}{t \sin 2i}$$

Hence the angular separation of the fringes increases with wavelength and approaching grazing emergence and also varies inversely as the plate thickness, the plate length having no influence. The dispersion of the instrument is found by differentiating (6), μ being a variable, and is given by the relation

$$(8) \quad \frac{\partial i}{\partial \lambda} = -\left[4t^2\mu \frac{\partial \mu}{\partial \lambda} - m^2\lambda\right] \Big/ 2t^2 \sin 2i$$

$$(9) \quad \frac{\partial i}{\partial \lambda} = \frac{2\lambda\mu \frac{\partial \mu}{\partial \lambda} - 2\left(\mu^2 - \sin^2 i\right)}{\lambda \sin 2i} .$$

From this the dispersion of the Lummer plate is evidently independent of the plate dimensions, it depends only upon the optical properties of the plate. If the Δi of (7) is equated to the Δi of (8) then the resulting $\Delta\lambda$ is

$$(10) \quad \Delta\lambda = \frac{m\lambda^2}{m^2\lambda - 4t^2\mu \frac{\partial \mu}{\partial \lambda}}$$ or is the difference in wavelength that a component must have in order that it coincides with the main fringe of the next order, this is the spectral range of the interferometer.

An exact expression for the resolving power of a Lummer plate is possible only at critical angle incidence in which case the Rayleigh criterion as to the smallest angle resolvable, δi - the angle between the central maximum and first minimum - may be applied. Since the wave front is of width $l\cos i$, δi is given by $\delta i \equiv \frac{\lambda}{l\cos i}$. From (9) is obtained a δi corresponding to a $\delta\lambda$ and hence equating gives

$$(11)\quad \delta i = -\frac{1}{\lambda \sin i \cos i}\,\delta\lambda\left\{\mu^2 - \sin^2 i - \lambda\mu\frac{\partial\mu}{\partial\lambda}\right\} \equiv \frac{\lambda}{t\cos i}$$

which means that $\delta\lambda$ is the smallest wavelength difference resolvable. The resolving power, defined as $\lambda/\delta\lambda$, is then

$$(12)\quad R.P. \equiv \frac{\lambda}{\delta\lambda} = \frac{t}{\lambda\sin i}\left[\mu^2 - \sin^2 i - \lambda\mu\frac{\partial\mu}{\partial\lambda}\right].$$

This is only true at grazing emergence since $\delta i \equiv \frac{\lambda}{t\cos i}$ only when the amplitude is uniform over the entire wave front of the partial waves. If $\sin i$ is taken as unity, valid since $90°-i$ is only $1°-2°$, then

$$(13)\quad \frac{\lambda}{\delta\lambda} \sim \frac{t}{\lambda}(\mu^2-1) \qquad \text{to a close approximation.}$$

The Lummer-Gehrcke plate interferometer is superior to the Fabry-Perot only in the ultraviolet region for here the reflecting power of metal films decreases greatly producing a large instrument fringe breadth and reduces the resolving power. However, the reflection coefficient of a quartz or glass surface remains high for all wavelengths provided incidence is near the critical angle and dictates use of a Lummer plate in this region.

In order to deduce the spectral line component separations from the Lummer plate fringes the reduction technique of Behrens[12] is employed. For simplicity only two components will be treated. The dispersion of the instrument is assumed to be parabolic as in the Fabry-Perot interferometer; the positions of two component fringes a_n and b_n in the n'th order produced by the spectral lines a and b are (arbitrary zero point)

$$a_m^2 = Am + B \qquad b_m^2 = A(m+\epsilon) + B$$

$$a_{m+1}^2 = A(m+1) + B \qquad b_{m+1}^2 = A(m+\epsilon+1) + B$$

where A and B are constants and ϵ is the fractional part of an order between a_m and b_m. From these

$$a_{m+1}^2 - a_m^2 = b_{m+1}^2 - b_m^2 = A$$

$$b_m^2 - a_m^2 = b_{m+1}^2 - a_{m+1}^2 = A\epsilon$$ which may be rewritten as

$$a_{m+1} + a_m = \frac{A}{a_{m+1} - a_m}, \quad b_{m+1} + b_m = \frac{A\epsilon}{b_m - a_m}.$$ Therefore

$$\epsilon = \frac{\epsilon(a_{m+1} + a_m) + \epsilon(b_{m+1} + b_m)}{(b_m + a_m) + (b_{m+1} + a_{m+1})}$$ which becomes

$$(14) \quad \epsilon = \left(\frac{1}{a_{m+1} - a_m} + \frac{1}{b_{m+1} - b_m}\right) \Big/ \left(\frac{1}{b_m - a_m} + \frac{1}{b_{m+1} - a_{m+1}}\right)$$

The actual wave number separation of the components is then

(15) $\delta\nu = \epsilon\,\Delta\nu$ where $\Delta\nu$ is the wave number difference between n'th and (n + 1) 'st order of interference. From 10, converting to wave numbers, $\Delta\nu$ is

$$\Delta\nu = \frac{m}{\frac{m^2}{\nu} - 4t^2\mu\frac{\partial\mu}{\partial\lambda}}$$ or closely enough

$$(16) \quad \Delta\nu = \frac{1}{2t}\frac{\sqrt{\mu^2 - 1}}{\left(\mu^2 - 1 - \mu\lambda\frac{\partial\mu}{\partial\lambda}\right)}$$. Hence measurement of the fringe component positions and knowledge of the Lummer plate optical properties allows calculation of component spectral line separations. Tolansky[13] gives methods of handling such calculations when a greater number of lines are present.

D. Summary

Resolving powers of upwards of 10^5 or 10^6 may be obtained with the Fabry-Perot type interferometer corresponding to resolving limits of the order of 0.005 cm^{-1} in the visible spectrum. The resultant interference fringes are easily and reliably reduced to give the structure separations. With quartz Lummer plates used in the ultraviolet resolving limits far below those of a Fabry-Perot are attainable although application to coarse structure is difficult due to problem of determining interference orders of the various fringe components.

For the high resolving powers necessary in hyperfine structure investigations either Fabry-Perot or Lummer plate interferometers may be employed, the decision as to which depending upon the ultimate resolving limit required and the spectral range.

V. General Theory of Hyperfine Structure

A. General.

Detection of spectral lines which were definitely not single but composed of a number of closely spaced lines pointed the need for introduction of a nuclear spin angular momentum vector, such fine structure having been proven not due to an isotope effect in all cases. Associated with such a nuclear spin is a magnetic moment - about 1/2000 'th that of an electron - and the resulting interaction between the magnetic moment and valence electrons would be expected to produce a splitting of the multiplet structure of the order observed. In addition to such evidence of a nuclear spin from atomic spectra, intensity alternation in the rotational structure of molecular band spectra in homonuclear molecules demanded that a nuclear spin $\vec{I}$ be introduced, $\vec{I}$ having the magnitude $\sqrt{I(I+1)}\ \frac{h}{2\pi}$ and I itself being integral or half integral only.

In order to determine the effect of a nuclear spin - actually the associated magnetic moment - upon the energy levels of an atom it is necessary to investigate the interaction of an arbitrary electron with such a nucleus. This interaction of electron and nucleus consists of two parts: 1) an interaction of electron orbit and nuclear spin and 2) an electron spin- nuclear spin interaction.

1. Spin orbit interaction.

Due to the orbital motion of the electron a magnetic field is produced at the position of the nucleus about which the nuclear magnetic moment precesses. This magnetic field is

(1) $\vec{H}_{orb} = \frac{\vec{\epsilon} \times \vec{v}}{c}$, $\vec{\epsilon}$ being the electric

field there produced by the orbital electron at a distance $\vec{r}$,

(2) $\vec{E} = \frac{e}{r^3}\vec{r}$. Hence

(3) $\vec{H}_{orb} = \frac{e}{c}\frac{\vec{r}\times\vec{v}}{r^3}$. The electronic orbital angular momentum is quantized and hence may take only those values

(4) $m\,\vec{r}\times\vec{v} = \vec{L}\frac{h}{2\pi}$ which with (3) gives

(5) $\vec{H}_{orb} = \frac{e}{mc}\vec{L}\frac{h}{2\pi}\left(\frac{1}{r^3}\right)$, m and e being the mass and charge of the valence electron. Since the nucleus has a magnetic moment $\vec{\mu}_I$, the ratio of magnetic to mechanical moments is

$\frac{\vec{\mu}_I}{\vec{I}\frac{h}{2\pi}} \equiv g_I\frac{e}{Mc}$ where g_I is the nuclear g factor and M the proton mass. Hence $\vec{\mu}_I$ is

(6) $\vec{\mu}_I = g_I\frac{eh}{4\pi Mc}\vec{I}$. The potential energy of this nuclear magnetic moment in the magnetic field produced by the electrons orbital motion, $\vec{H}_{orb}$, is

(7) $V_{orb} = \vec{H}_{orb}\cdot\vec{\mu}_I$ or

(8) $= g_I\left(\frac{eh}{4\pi Mc}\right)2\left(\frac{eh}{4\pi mc}\right)\left(\frac{1}{r^3}\right)\vec{L}\cdot\vec{I}$.

Recalling that the nuclear and Bohr magnetons are defined by

(9) $\mu_N \equiv \frac{eh}{4\pi Mc}$, $\mu_B \equiv \frac{eh}{4\pi mc}$, then

$$V_{orb} = 2g_I\frac{\mu_N\mu_B}{r^3}\vec{L}\cdot\vec{I}$$

(10) $V_{orb} = a\,\vec{L}\cdot\vec{I}$

2. Spin-spin interaction

Recalling that with the nuclear and electronic spin angular momenta are associated a nuclear and electronic magnetic moment, the spin-spin interaction is essentially the interaction of two magnetic dipoles $\vec{\mu}_I$ and $\vec{\mu}_s$ where $\vec{\mu}_s$ is the electronic magnetic moment. This dipole interaction is of the form[14]

$$(11) \quad V_{dipole} = -\left[\frac{3\vec{\mu}_s\cdot\vec{r}\;\vec{\mu}_I\cdot\vec{r}}{r^5} - \frac{\vec{\mu}_s\cdot\vec{\mu}_I}{r^3}\right]$$

The magnetic moments $\vec{\mu}_I$ and $\vec{\mu}_s$ are given, in terms of the nuclear and Bohr magnetons, by

$$(12) \quad \vec{\mu}_I = g_I \mu_N \vec{I}$$

$$\vec{\mu}_s = -2\mu_B \vec{s}$$

and hence (11) becomes

$$V_{dipole} = 2 g_I \frac{\mu_N \mu_B}{r^3}\left[\frac{3\vec{I}\cdot\vec{r}\;\vec{s}\cdot\vec{r}}{r^2} - \vec{I}\cdot\vec{s}\right]$$

$$(13) \quad V_{dipole} = 2a\left[\frac{3\vec{I}\cdot\vec{r}\;\vec{s}\cdot\vec{r}}{r^2} - \vec{I}\cdot\vec{s}\right] .$$

Hence the total interaction between a nucleus of spin $\vec{I}$ and a single valence electron is

$$(14) \quad V_{total} = a\,\vec{L}\cdot\vec{I} + 2a\left[\frac{3\vec{I}\cdot\vec{r}\;\vec{s}\cdot\vec{r}}{r^2} - \vec{I}\cdot\vec{s}\right]$$

where a is $a \equiv g_I \frac{\mu_N \mu_B}{r^3}$. This rather cumbersome expression is equivalent to one of the form

$V_{Total} = a_J\,\vec{I}\cdot\vec{J}$. Recalling that the quantum mechanical average of a vector, $\vec{L}$ for instance, in the direction of another vector, say $\vec{J}$, is just the component of $\vec{L}$ along $\vec{J}$ if $\vec{L}$ precesses about $\vec{J}$. From the diagram the magnitude of the component

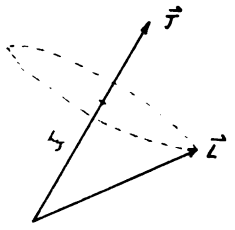

of $\vec{L}$ along $\vec{J}$ is

$$L_J = \frac{\vec{L}\cdot\vec{J}}{|\vec{J}|}$$

and since the unit vector along $\vec{J}$ is $\frac{\vec{J}}{|\vec{J}|}$, then $\langle \vec{L} \rangle_{av} = \frac{\vec{L}\cdot\vec{J}}{J(J+1)}\vec{J}$ where J^2 has been replaced by $J(J+1)$. Using this result then, (10) becomes

$$(15)\quad V_{nl} = a\,\vec{L}\cdot\vec{I} = a\,\frac{\vec{L}\cdot\vec{J}}{J(J+1)}\,\vec{J}\cdot\vec{I} = \frac{a}{2J(J+1)}\left[J(J+1)+L(L+1)-S(S+1)\right]\vec{J}\cdot\vec{I}.$$

Bethe[15] shows that (13) reduces to the form

$$(16)\quad V_{dipole} = \frac{-1}{(2L+3)(2L-1)J(J+1)}\left[\frac{3}{2}\left\{J(J+1)-L(L+1)-S(S+1)\right\}\left\{J(J+1)+L(L+1)-S(S+1)\right\} - L(L+1)\left\{J(J+1)+S(S+1)-L(L+1)\right\}\right]\vec{I}\cdot\vec{J}$$

and hence the total interaction, V_{Total}, is

$$(17)\quad V_{Total} = a_J\,\vec{I}\cdot\vec{J} \qquad \text{where}$$

$$a_J = \frac{a}{2J(J+1)}\left[J(J+1)+L(L+1)-S(S+1)\right] - \frac{a}{(2L+3)(2L-1)J(J+1)}\cdot$$

$$\left[\frac{3}{2}\left\{J(J+1)-L(L+1)-S(S+1)\right\}\left\{J(J+1)+L(L+1)-S(S+1)\right\} - L(L+1)\left\{J(J+1)+S(S+1)-L(L+1)\right\}\right]$$

B. Hyperfine structure in Cu.

The most important cases of this interaction - those in which the simplest expression for V_{Total} is obtained - are

1. **S states.** $L = 0$ and $J = S$ and hence

$$(18)\quad a_J = 0$$

and no hyperfine structure results.

2. $S = 1/2$. For both $J = L + 1/2$ and $J = L - 1/2$,

$$(19) \qquad a_J = \frac{L(L+1)}{J(J+1)}\, a$$

An application of these theoretical results will be made to the hyperfine structure of the $^2D - {}^2P$ triplet in copper and an attempt to verify such structure using a hollow cathode discharge source with both Fabry-Perot and Lummer-Gehrcke plate interferometers as resolving instruments will be described.

Copper in both of its isotopic forms, Cu^{63} and Cu^{65} , have a nuclear spin $I = 3/2$ [16] and as a result the multiplet levels $^2P_{3/2}$, $^2P_{1/2}$, $^2D_{3/2}$ and $^2D_{5/2}$ are split into hyperfine structure levels by the interaction of nuclear spin and valence electron. The resulting energy levels may be calculated from (17) where a_J is defined by (19). Using these relations Table 2 is obtained in which the term change is given as a function of the interaction constant a . In Figure 9 is depicted the energy level splitting and the resultant hyperfine structure transitions in the triplet. This diagram is drawn to give the number of components, row a, and the resulting simplification gained by assuming that the ^2P level splitting constants are zero, row b.

Existence of an isotope results in a greater complexity of the observed hyperfine structure. There are hyperfine structure components produced for each of these isotopes Cu^{63} and Cu^{65} , the separations being slightly different and the entire group of each being displaced. Whereas with a single isotope the hyperfine structure should appear as in Figure 9 the presence of an additional isotope and the accompanying components make resolution of individual line difficult.

Table 2. Term value shift as function of interaction constant

Multiplet level	a_j	F and corresponding V values				
$^2P_{3/2}$	$\frac{8}{15}a_1$	F	3	2	1	0
		V	$\frac{6}{5}a_1$	$-\frac{2}{5}a_1$	$-\frac{22}{15}a_1$	$-2a_1$
$^2P_{1/2}$	$\frac{8}{3}a_1$	F	2	1		
		V	$2a_1$	$-\frac{10}{3}a_1$		
$^2D_{3/2}$	$\frac{8}{5}a_2$	F	3	2	1	0
		V	$\frac{18}{5}a_2$	$-\frac{6}{5}a_2$	$-\frac{22}{5}a_2$	$-6a_2$
$^2D_{5/2}$	$\frac{24}{35}a_2$	F	4	3	2	1
		V	$\frac{18}{7}a_2$	$-\frac{6}{35}a_2$	$-\frac{78}{35}a_2$	$-\frac{18}{5}a_2$

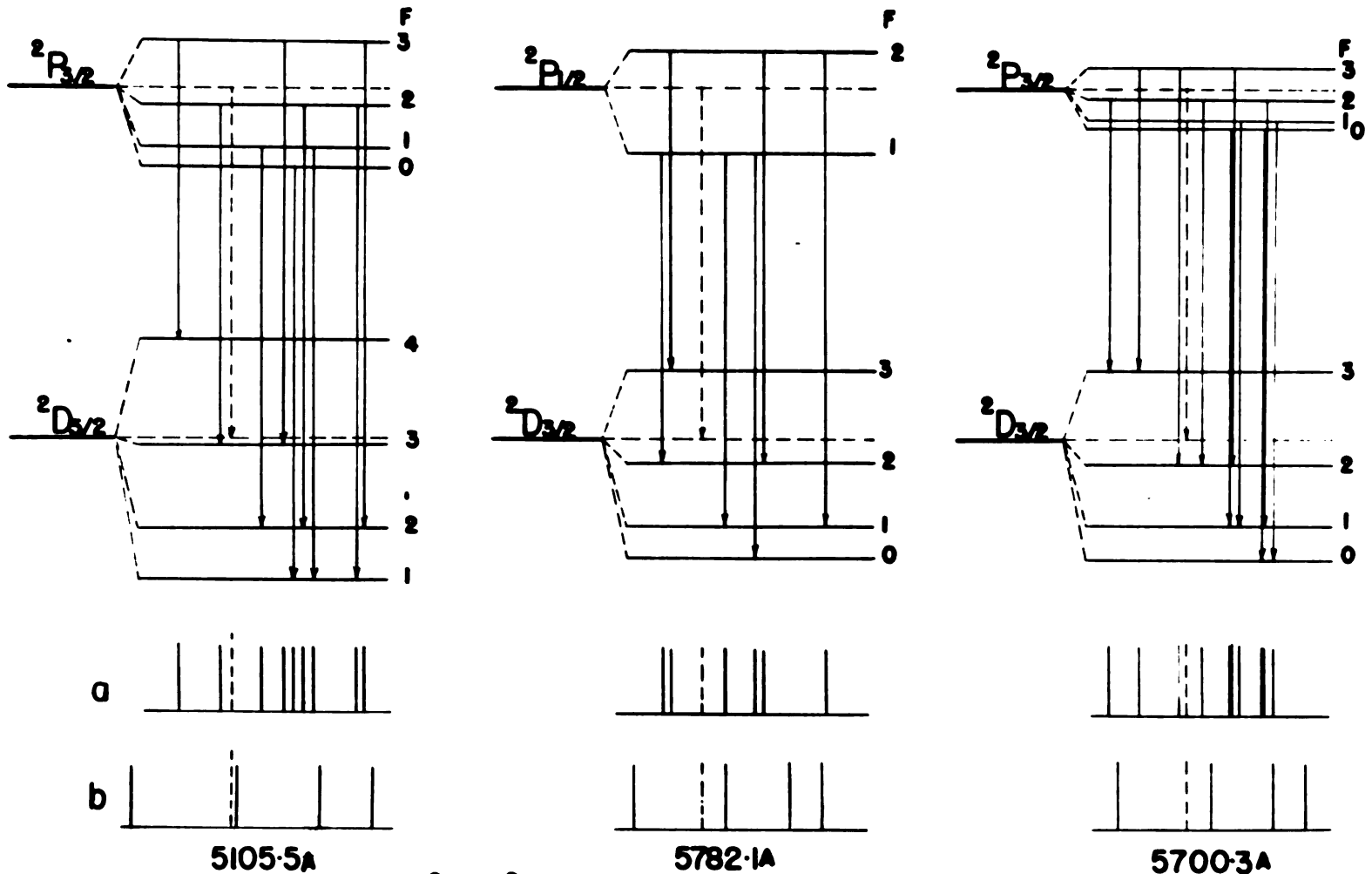

FIGURE 8 Hyperfine Structure of $^2P - {}^2D$ Triplet in Copper.
One isotope only

VI. Experimental

A. Optical system.

Radiation emanating from the hollow cathode is collimated and the direction of propagation changed from vertical to horizontal by means of a first surface Aluminum mirror. Such collimated light is then incident on a Fabry-Perot interferometer, aperture of 1 cm. and plate separation of 10.1599 mm, and the emergent radiation is focussed on the entrance slit of a Hilger Constant Deviation Spectrometer. By tilting the etalon, rotating it about a horizontal axis parallel to the plane of the slit, the maximum of intensity is placed at the position of the second or third fringe and observations were possible, visual and photographic. A 4.56 mm glass Lummer-Gehrcke plate was also used as a resolving instrument, the optical train being identical although tilting of this instrument may introduce ghost images which will appear to be structure. With the plate in a horizontal plane and using the same focussing lens only the first two orders of interference on either side of the center were available for observation. In the figure is a photograph of the optical system with the Lummer plate in position.

The resulting interference fringes were photographed with a plate camera, the camera lens being placed adjacent to the spectrometer eyepiece; focusing was facilitated by viewing the fringes on the camera ground glass plate with an eyepiece. Interference fringe size on the photographic plates was controlled by the camera magnification and was set so as to allow reasonable exposure times and yet have the fringes far enough separated so that measurement of fringe separations was possible. Kodak Spectroscopic Plates III-F3, 3 1/4 x 4 1/4 were used

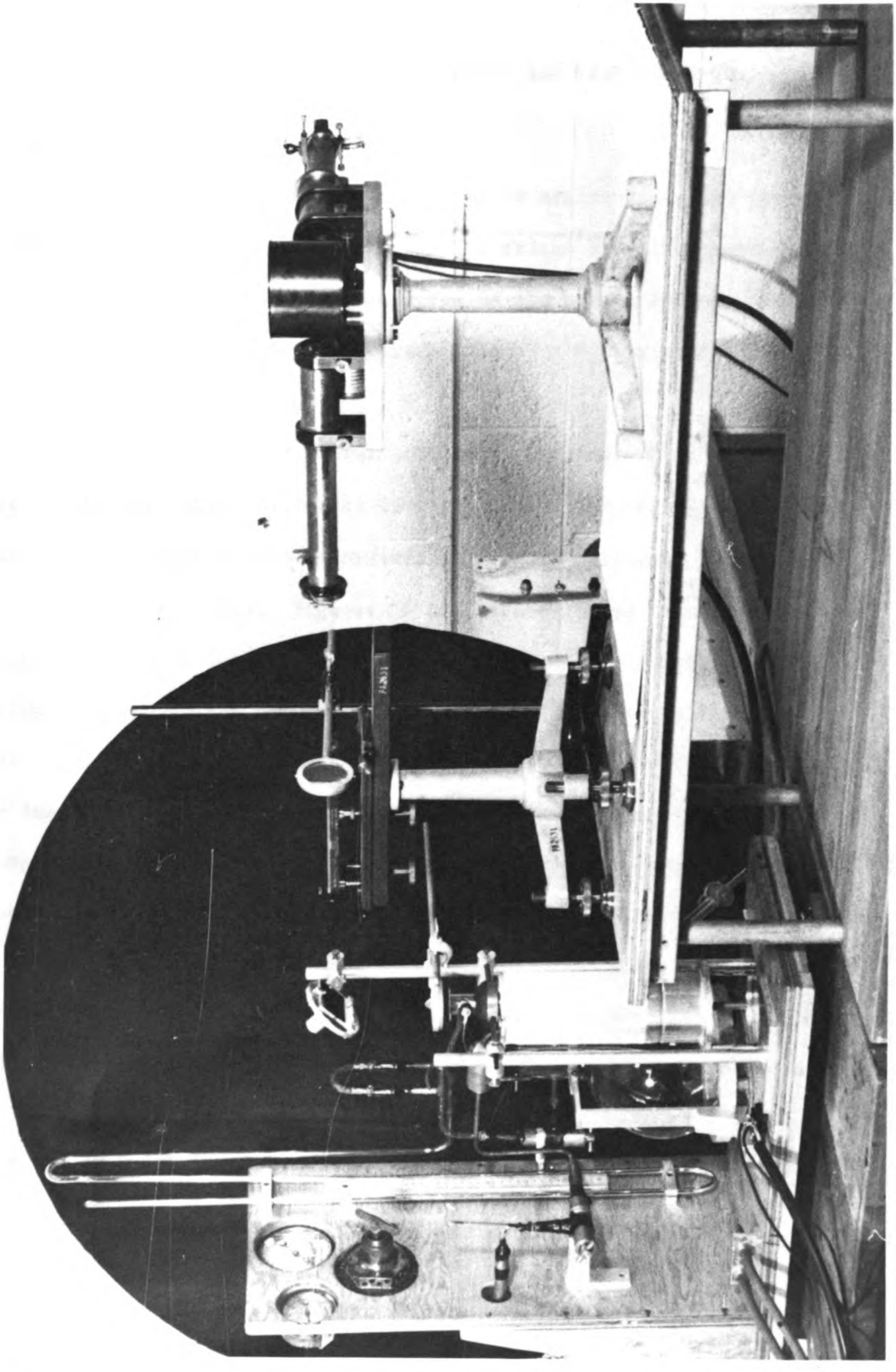

and were developed in D-19 for 3 1/2 minutes and fixed in D-76.

B. Results of investigation.

The results of this problem will be discussed in two parts. First the preliminary investigation of the fringe breadth, hence directly the spectral line breadth, as influenced by the hollow cathode source and secondly the hyperfine structure of the $^2D - ^2P$ triplet in Cu.

1. Line breadth

The interference patterns obtained for the $^2D - ^2P$ triplet were repeated at three different temperatures of the refrigerant: cold water, solid CO_2 and acetone mixture and liquid nitrogen, 15°C, - 78°C and -195°C respectively. Figures 10 and 11 show these fringes and a comparison of identical fringes at different temperatures is possible. Making this comparison between fringe breadths temperature reduction is seen to increase fringe sharpness, decrease the fringe width. Since the instrumental contribution to fringe width is constant over each group of fringe patterns and the gas pressure and tube current are constant, the conclusion is that lower temperatures give a reduction in the spectral line width, this being characteristic of the doppler effect broadening of lines. At liquid nitrogen temperature the expected natural doppler and collision breadths are

1. natural $\sim$ .0002 cm^{-1}
2. doppler $\sim$ 0.016 cm^{-1}
3. collision $\sim$ 0.002 cm^{-1}

It is to be noted among the interference fringe patterns that the tube current for the Lummer plate analysis at liquid nitrogen

Figure 10 Fabry-Perot Interference Fringes

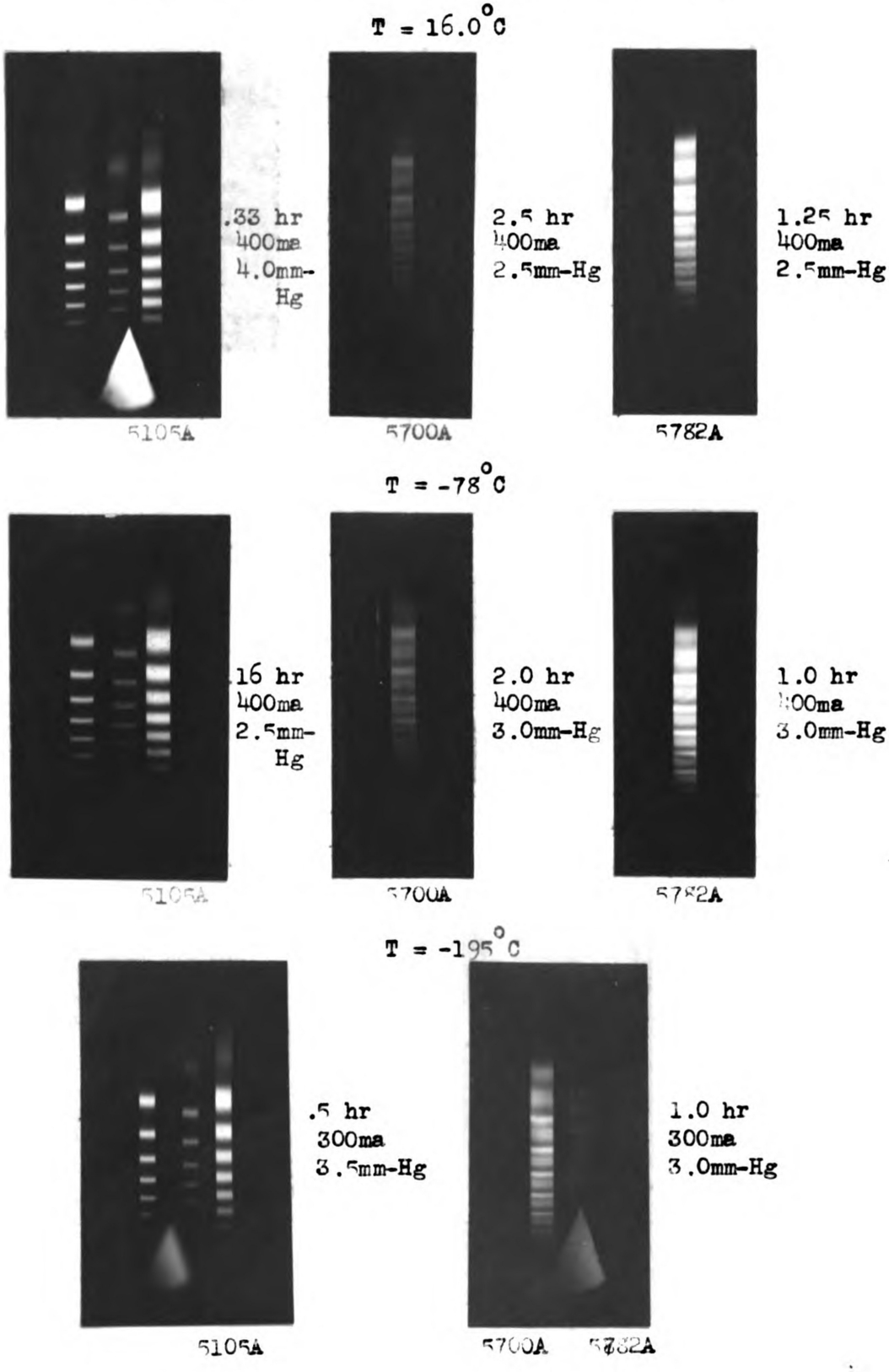

Figure 11 Lummer-Gehrcke Interference Fringes

$T = 16.0^{\circ}C$

5105A

.16 hr
300ma
2.5mm-Hg

5700A 5782A

.33 hr
300ma
2.5mm-Hg

$T = -78^{\circ}C$

5105A

.08 hr
300ma
2.5mm-Hg

5700A

1.0 hr
400ma
2.5mm-Hg

5782A

.33 hr
400ma
2.5mm-Hg

$T = -195^{\circ}C$

5105A

.16 hr
150 ma
2.5mm-Hg

5700A

2.5 hr
150ma
2.5mm-Hg

5782A

1.0 hr
150ma
2.5mm-Hg

temperature has been reduced to 150 ma, this reduction in current giving a lower intensity but serving to increase the fringe sharpness. With the Fabry-Perot etalon such currents gave intensities lower than were practicable to use and hence higher currents had to be used. This effect was not photographed but was noted visually with the spectrometer. Since all other conditions were identical, the conclusion reached is that lower tube currents give rise to sharper spectral lines; this effect is just that to be expected on the basis of stark effect broadening of spectral lines.

Confirmation of pressure and collision broadening effects were not obtained due to the limited range of pressures within which the discharge tube operated correctly, 1 - 5 mm Hg. Within this range of pressures such broadening effects would not be apparent visually and probably not photographically.

2. Hyperfine structure of Cu.

From the interference patterns obtained when the hollow cathode source was operated at -195°C the number of hyperfine structure components and their separations were calculated. The Fabry-Perot fringes allowed such a determination to be made for the 5700 and 5782 Å lines, the 5105Å being unresolved. With the Lummer plate patterns the hyperfine structure was deduced for all of the triplet lines.

The negatives were analyzed by measuring the fringe positions with a traveling microscope (least count of 0.005 mm), the settings of pointer on fringe center being made with the unaided eye. Two separate measurements were made and the fringe intervals agreed to within 0.02 mm for the majority of cases. Using these fringe separations the component

intervals were calculated using Behren's method of reduction for the Lummer-Gehrcke plate patterns and a similar method[17] for the off-center Fabry-Perot fringes. The results of these calculations are summarized in the following tables.

a) Using Fabry-Perot etalon.

Transition	λ	Components	Component separations	
	A		cm^{-1}	
$^2D_{5/2} - {}^2P_{3/2}$	5105.55	Not resolved		
$^2D_{3/2} - {}^2P_{3/2}$	5700.25	3	.181	.091
$^2D_{3/2} - {}^2P_{1/2}$	5782.13	3	.171	.099

b) Using Lummer-Gehrcke plate

Transition	λ	Components	Component separations	
	A		cm^{-1}	
$^2D_{5/2} - {}^2P_{3/2}$	5105.55	3	.091	.083
$^2D_{3/2} - {}^2P_{3/2}$	5700.25	3	.148	.119
$^2D_{3/2} - {}^2P_{1/2}$	5782.13	5	.072	.097
			.108	.075

Examination of Figure 12 in which the hyperfine structure groups are compared with those predicted and observed by Ritschl, Zeitschrift fur Physik 79, 1 (1932), and Schuler and Schmidt, (Zeitschrift fur Physik 100, 113 (1936), reveals that the resolving limit of the Fabry-Perot etalon was not low enough, no components being resolved in the 5105A and only three each in the 5700A and 5782A groups. This lack of resolving power is due to the fact that the Al film was thinner than required; this was used in the interests of sufficient fringe intensity. The resolving

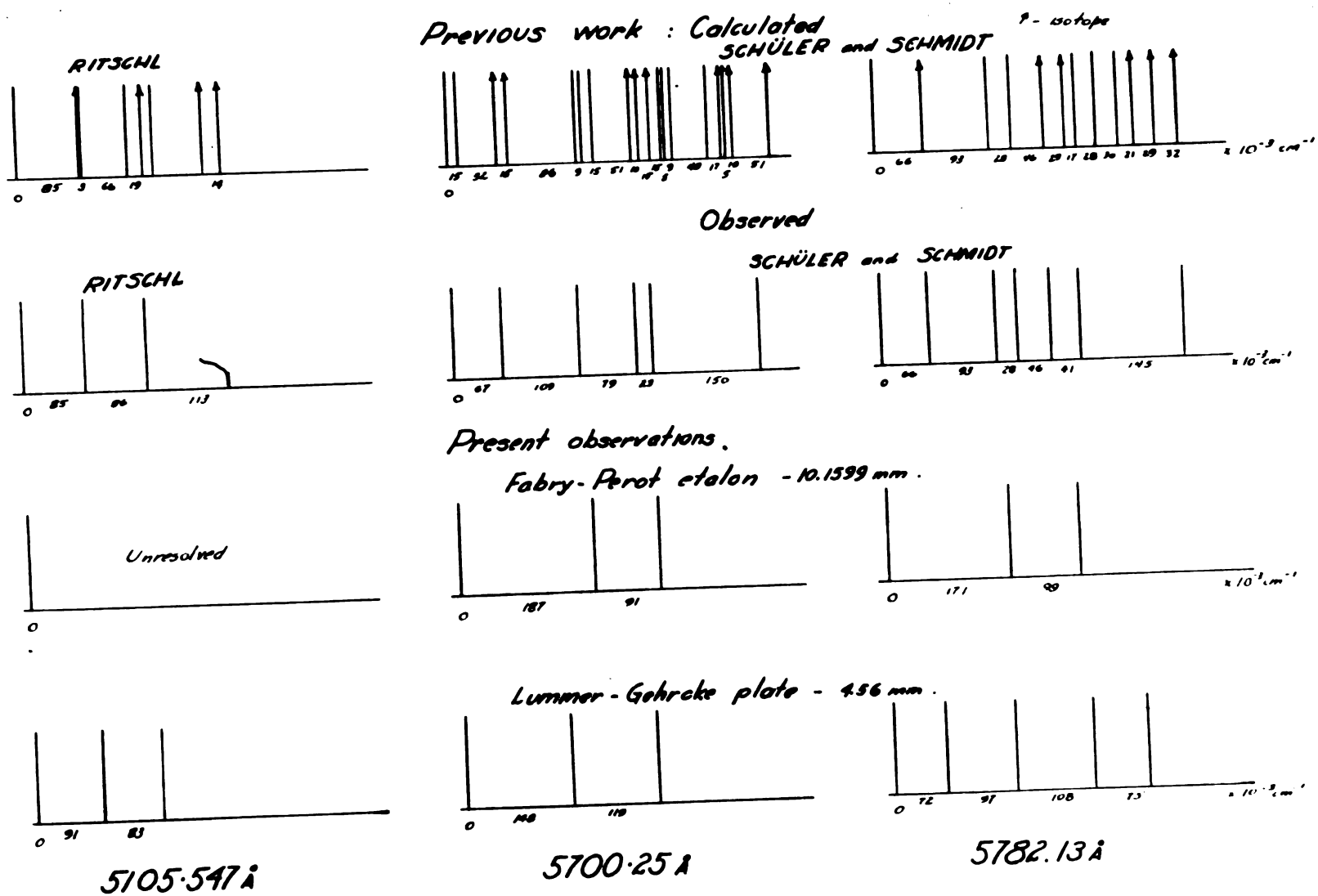
Previous work : Calculated
RITSCHL
SCHÜLER and SCHMIDT
9 - isotope
Observed
RITSCHL
SCHÜLER and SCHMIDT
Present observations.
Fabry-Perot etalon - 10.1599 mm.
Unresolved
Lummer-Gehrcke plate - 4.56 mm.
5105·547 Å
5700·25 Å
5782.13 Å

Figure 12

limit of a Fabry-Perot etalon depends directly upon the surface film reflection power; with a 1 cm etalon a resolving limit of 0.062 cm^{-1} is possible with 70 per cent reflecting surfaces and increasing this to 95 per cent reduces the resolving limit to 0.008 cm^{-1}, theoretically. Hence with the etalon used, 1.01599 cm separation, the hyperfine structure of these three Cu lines should be capable of resolution with a reasonably high reflecting film. However, such films reduce the fringe intensity to the point where, with this experimental arrangement at least, the necessary exposure time is impractical. The conclusion is then that unless larger etalon separations are used with these lower reflecting power films, this hyperfine structure is not resolvable.

With the glass Lummer plate the resolution was sufficient to give three hyperfine components in the 5105A and 5700A groups and five in the 5782A one. The component intervals for the 5105A group are very nearly those observed by Schuler and Schmidt. The separations of the 5782A set are also closely those reported. Since here the third through seventh calculated components have different intensities and the observed lines represent the resultant intensity distribution maxima, the agreement with theory is fair. In the 5700A group, as calculated, the intensities range from 3 to 100 and the resulting distribution would be expected to have maxima between the first and second clusters of lines, about the third cluster and again for the fourth. The last group have very low intensities and probably are not detectable. On this basis the maxima intervals would correspond roughly to those observed. Why these lines of 0.060 to 0.080 cm^{-1} intervals are not separated here as they are in the 5782A structure is a puzzle. Lower resolving limits with this

Lummer-Gehrcke plate are possible by using angles of incidence nearer the critical angle and by using only the perpendicular component of the light since the reflecting power of a surface is higher for this than for the parallel component at a given angle of incidence. This possibility has not been explored as yet.

Although hyperfine structure intervals are quoted to 0.001 cm^{-1} the last figure is uncertain due to the closeness of the fringe components and to the method of measuring fringe separations. Therefore these structure intervals must be viewed with a degree of caution.

VII. Conclusion.

A hollow cathode discharge source has been designed and constructed with which the spectral line breadths and the hyperfine structure in copper have been investigated. Temperature dependence of this line breadth and also a dependence upon discharge tube current have been noted; these effects being those expected on the basis of Doppler and Stark effect broadening. Using both Fabry-Perot and Lummer-Gehrcke plate interferometers as resolving instruments the hyperfine structure of the $^2D - ^2P$ multiplet in copper have been observed, the resultant structure intervals as obtained from the Lummer plate fringes being in general agreement with previous observations. No determination of the appropriate interaction constants is possible due to incomplete resolution.

Due to the possibility of producing spectral lines of narrow breadth this type source could find application in

1) Investigation of spectral line breadths themselves and quantitative measurements of line breadth dependence upon gas pressure, discharge tube current and temperature;
2) analysis of hyperfine and isotope structure in spectral lines using the techniques employed here; and
3) production of molecular band spectra, particularly ionized diatomic molecules, for purposes of rotational and vibrational analysis.

REFERENCES

1. Margenau, H. and Watson, J. Rev. Mod. Phys. 8, 22 (1936)

2. White, H. Introduction to Atomic Spectra (McGraw-Hill, 1933) p. 419

3. Margenau, H. Phys. Rev. 82, 156 (1951)

4. Holstein, T. Phys. Rev. 79, 744 (1950)

5. Margenau, H. Phys. Rev. 82, 156 (1951)

6. Born, M. Optik (Springer, 1933)

7. Paschen, F. Ann der Physik 50, 901 (1916)

8. Schuler, H. Zeits. fur Physik 35, 323 (1926)

9. Arroe, M. and Mack, J. J. O. S. A. 40, 387 (1950)

10. McNally, J., Harrison, G. and Rowe, E. J. O. S. A. 37, 93 (1947)

11. Tolansky, S. High Resolution Spectroscopy (Pitman, 1947)

12. Behrens, D. J. Journ. Sci. Instru. 18, 238 (1941)

13. Tolansky, S. High Resolution Spectroscopy (Pitman, 1947) p. 211

14. Weatherburn, C. E. Advanced Vector Analysis (Bell, 1944) p. 161

15. Bethe, H. Handbuch der Physik vol. 34/1 p. 557

16. Mack, J. E. Rev. Mod. Phys. 22, 64 (1950)

17. Tolansky, S. High Resolution Spectroscopy (Pitman, 1947) p. 133